P-29

NUMERICAL INVESTIGATIONS IN THREE-DIMENSIONAL INTERNAL FLOWS

SEMI-ANNUAL STATUS REPORT

1 JANUARY THROUGH 30 JUNE 1990

Prepared for:

NASA-AMES RESEARCH CENTER

MOFFETT FIELD, CA 94035

UNDER NASA GRANT

NCC 2-507

By:

WILLIAM C. ROSE

ENGINEERING RESEARCH AND DEVELOPMENT CENTER

UNIVERSITY OF NEVADA, RENO

RENO, NV 89557

I. BACKGROUND

During the course of the present Grant, numerical simulations of various three-dimensional (3D) flow fields have been carried out. Some of these flow fields have been for inlets, while others have been for nozzles. These classes of flows have been investigated primarily in the supersonic region and have concerned themselves with models of various parts of propulsion devices, either tested or to be tested in ground-based facilities. The current effort takes a slight change from the previous efforts while still concentrating on the three-dimensional flow in nozzles.

The flow in the NASA-Ames 11-ft transonic test facility was investigated using the three-dimensional Computational Fluid Dynamics (CFD) techniques developed and pursued throughout the present Grant. The application of CFD to investigating the flow within ground-based facilities has not been exploited to any great degree, and yet this technique holds a large promise for being able to determine potential problems in these facilities. Further, the CFD could lead to methods to improve on the flow quality or alleviate existing major problems within flow facilities. In the closed loop wind tunnel, some portions of the flow are more amenable to numerical analysis than others. For example, flows involving rapid rates of diffusion, whether they be supersonic or subsonic, are typically difficult to model accurately through CFD. This is true because the flow physics involving the turbulence in the presence of large adverse pressure gradients or potential boundary layer separations is not well understood, thus the computational results are always subject to uncertainties due to these limitations. On the other hand, for accelerating flows such as those in the contraction sections of subsonic wind tunnels, fluid physics is relatively well understood and it is known that boundary layers in these environments are relatively easy to calculate.

The remainder of this report discusses the application of the full Navier-Stokes (FNS) 3D code to the flow qualities in the contraction section of the NASA-Ames 11-ft transonic wind tunnel.

II. INTRODUCTION

In recent years, aerodynamic testing of various airfoil shapes has taken on a new dimension of criticality with respect to the flow quality involved in the test facilities used. In the NASA-Ames 11-ft wind tunnel, discrepancies in the flow quality, that is flow uniformity and flow angularity within the test section, have been observed. The magnitudes of these flow irregularities have been debated since they are difficult to measure. In the 11-ft tunnel, the asymmetrical contraction and the transition section from the circular settling chamber to the square test section are potential sources of flow irregularities. Of particular concern is the possibility for the introduction of secondary flows within the contraction section. In a previous study (carried out under another program), the nature of the contraction in the 11-ft tunnel has been investigated. In that study, particular interest in whether or not sudden changes in the contraction geometry (as it currently exists) have the potential to introduce flow separation and possible unsteadiness. A brief summary of the results of that study is discussed here.

The approach taken in the previous study was to use the two-dimensional full Navier-Stokes equations to investigate the flow along two specific flow paths within the three-dimensional contraction section. Although this is an approximation that may or may not be warranted depending on the objectives of the calculations, it is reasonable for purposes of determining whether or not separations could exist. Two paths representing the full range of expected pressure gradients were chosen. The first is a cut along the vertical plane of symmetry through the 11-ft contraction. The other section chosen for investigation is a hypothetical section, consisting of the contours along what is to become one of the corners of the test section. This includes a fairing plate that is located along the transition between the circular cross section and the square cross

section. The first of these trajectories along the vertical symmetry plane was treated as a planar two-dimensional flow, while the corner path is treated as though it were an axially symmetric flow. Because of the way the contraction is constructed, geometric changes occur at different streamwise axial positions throughout the contraction on these two different trajectories.

The results of the previous study indicated that little, if any, significant separation is likely to occur. However, because of the aforementioned differences in the location of the geometric changes, the locations of the pressure gradients that were found to exist differed substantially from the vertical symmetry plane to the corner flow. This situation is known in certain cases to lead to significant lateral flows, possibly leading to severe secondary flows. Such secondary flows were observed during the present Grant for the supersonic nozzle calculations done for the NASA-Ames 100 MW arc heater.

In general, there are two primary sources of secondary flow. The secondary flow observed in the supersonic nozzle calculation (and expected to be likely to occur in the NASA-Ames 11-ft wind tunnel) is in the general category of inviscidly induced secondary flows. The meaning of this is that the inviscid pressure gradients associated with geometry changes cause lateral pressure gradients to exist in the flow. Little, if any, secondary flow would exist if the flow were actually inviscid. However, when these pressure gradients are allowed to act on flow that is viscous, such as in a real nozzle, they act through the low momentum portions of the boundary layer to potentially produce very large flow angularity. This flow angularity, in combination with the primary axial flow in the contraction, leads to secondary flows. The other type of secondary flow is that associated with the existence of corners in which turbulent boundary layers are growing. Because of certain constraints on the Reynolds stress variation throughout the

corner flow, cellular secondary flows are produced. These flows are expected to be difficult, if not virtually impossible, to calculate since no CFD method has ever been demonstrated to given valid results for this type of secondary flow. As a result of this latter situation, these flows are not discussed further in this study. In contrast to the latter Reynolds stress-induced corner flows, the inviscidly driven secondary flows, as previously noted, have been found in full three-dimensional CFD results, and, in addition, have been shown to exist experimentally in these nozzles.

The two-dimensional results completed previously have shown that the surface pressure ratio, that is the ratio of the static pressure on the surface of the contraction relative to that in the settling chamber varies depending on what "2D" trajectory was taken through the contraction section. Figure 1 summarizes these results for the solution along the vertical symmetry plane and along the diagonal axially symmetric plane. Both results are from the SCRAM2D code. The results are shown for the diagonal cut with a solid line and for the vertical symmetry cut with a dashed line. The contraction is initiated sooner on the vertical symmetry plane than along the diagonal, producing a lowering of the surface pressure along that wall sooner than on the diagonal cut. The net result is a situation that has the potential to produce the inviscidly driven secondary flow discussed above.

Whether or not the full 3D simulations will demonstrate this variation in pressure ratio along various trajectories in the contraction and show secondary flow is the subject of this study.

III. RESULTS AND DISCUSSION

III.1 Grid Generation

The SCRAM3D code used throughout this Grant assumes the existence of multi-faceted walls and does not explicitly handle polar coordinates. Thus, a grid must be generated to model the contraction that fits within the capability of the existing code and yet has a sufficient fidelity to model the flow behavior. The transition from a full circular cross section to a square cross section must accurately represent the geometry so that the pressure gradients are accurately modeled. For purposes of this study, the solution was assumed to start from the innermost wall of the 11-ft settling chamber. The behavior of either the core flow or the boundary layer flow in the vicinity of the origin of the settling chamber is unknown, however, for purposes of discussion, this initially uniform flow will represent a best case analysis in terms of investigating the origin of secondary flow for the contraction section alone. In order to generate a grid compatible with SCRAM3D, the cylindrical section of the contraction is modeled as a twelve-sided surface. The remainder of the contraction is modeled from the equations provided by NASA personnel. The actual contraction section in the wind tunnel has a symmetry plane located between the upper and lower halves of the tunnel. The grid is thus modeled as a symmetry grid, and only the flow in the lower half of the tunnel is computed. Streamwise locations of the grid intersections are every one foot along the 85 feet of flow calculated here. This flow contains the entire contraction section plus a substantial amount of the test section. The grid walls chosen for this study are shown in Figure 2. This is a view of the lower half of the walls of the contraction section looking downstream into the test section. The grid is condensed along the intersections that are to become corners of the test section. This is done to allow better resolution

of the boundary layers along the walls in the region where secondary flow effects are most likely to be seen. One of the lower corners highlighted through the denser grid corresponds to the corner trajectory discussed above in the two-dimensional calculations, while the vertical symmetry plane trajectory location discussed for the 2D calculations is located along the center of Figure 2. A representative cross flow plane showing compaction and general arrangement of the grid is shown in Figure 3. The entire grid is 85 streamwise points by 34 points located from the symmetry plane of the solution to the opposite wall and 65 points from the left sidewall to the right sidewall.

It should be noted in Figures 2 and 4 that the top and bottom of the contraction section achieve their final total 11-foot height well ahead of that associated with the sidewall contraction. This is due to the requirement for flat surfaces in order to allow the flexible sidewalls to operate. This also provides the driving mechanism for the possible secondary flow.

In order to facilitate presentation of the flow solutions in the present study, the left hand sidewall was removed from the grid and the perspective point was moved slightly to the interior of the tunnel circuit and downstream of that shown in Figure 2. The geometry is shown in Figure 4. The results of the flow solution are shown either along the surfaces or through the center planes of the grid as discussed in the following section.

III.2 Flow Solution

Flow solutions are depicted in this study in terms of the local Mach number and pressure ratio. The Mach number contours on the two center planes from the solution are shown in Figure 5. Here the blue shading indicates lower Mach numbers

while the red indicates higher Mach numbers. Figure 5 shows the overall trend of acceleration through the contraction section. An enlargement of the solution near the end of the contraction section is shown in Figure 6. It is clear that slight variations in the Mach number occur within any given cross flow plane through the contraction. For example, in Figure 6, the flow near the sidewall remains slightly slower than that near the vertical center plane as evidenced by the slightly different shading. In contrast, slightly higher Mach numbers are observed on the sidewall near the final sidewall contraction. This asymmetry in Mach number arises from the contraction asymmetry discussed above. The normalized pressure for the solution is depicted in Figure 7 for the horizontal (solution) symmetry and the vertical symmetry planes. An enlargement of this figure is shown in Figure 8 and also reveals the point discussed with respect to Figure 6 concerning the acceleration on the upstream part of the bottom wall. For Figures 7 and 8, the shading is from red, a higher pressure, to blue, a lower pressure, as one goes through the contraction section. This group of figures have shown the results for Mach number and pressure ratio obtained on the center planes of the tunnel. The surface pressure distributions are also of interest. Figure 9 shows the normalized surface pressure distribution throughout the contraction section. The slight asymmetries, again, are evident, showing a lower pressure on the bottom wall of the solution relative to the sidewall in the forward portion of the contraction, while the situation is reversed near the end of the sidewall contraction. In another portrayal of the normalized pressure, Figure 10 shows the pressure ratio contours in six representative cross flow planes. The third and fifth cross flow planes demonstrate locations of lateral pressure variations within a given cross flow plane.

III.3 Comparison with 2D Solutions

The results of the simulation of the 11-ft contraction wind tunnel with the 3D code with respect to pressure variations throughout the contraction can be summarized as follows. Recall Figure 1 that showed the differences between pressures obtained in two planes using SCRAM2D. A large difference in the pressure gradient was seen. The results of the present 3D calculations can be summarized as shown in Figure 11. The solutions from Figure 1 are repeated here, and, in addition, five representative trajectories from the 3D solution are shown for comparison. As is evident, the three-dimensional solutions: (1) are virtually all the same, and (2) agree quite well with the diagonal-cut axially symmetric solution from the 2D code. This indicates that the vertical-cut symmetry plane two-dimensional solution does not represent the full three-dimensional nature of the contraction. The results seem to dismiss the argument that large secondary flows could be expected to arise because of the inviscidly driven potential associated with large differences in pressure gradients occurring along different trajectories through the contraction section. However, as noted above, some lateral pressure variations do exist and the issue of secondary flow is investigated further in the next section.

III.4 Secondary Flow Investigation

The solution can be used to determine the paths taken by particles throughout the velocity field. These so-called "particle traces" are useful for ascertaining the trajectory of hypothetical particles released in the upstream portion of the solution. Figures 12 and 13 show the top view and side view, respectively, of particles released in the upstream portion of the contraction. No significant deviation from the expected

trajectories is seen. Figure 14 shows a detail of the contraction corner just after the bottom wall has become flat. Near the outflow boundary, a slight amount of helical flow can be observed, although its apparent magnitude in this figure is quite small. Velocity vectors near the end of the solution within the test section can be used to demonstrate the nature of the secondary flow that can be expected to occur within the 11-foot test section. Figure 15 shows a velocity vector plot where both the vector length and color are proportional to the magnitude of the cross flow velocity. The magnitudes of the velocity vectors are everywhere less than about 1% of the settling chamber value, indicating that although secondary flows exist in the cross flow plane, their magnitude is not large. The swirl, that is the cross product of the cross flow velocity vector and the streamwise vector, is shown in Figure 16. This indicates that large swirls occur only within the boundary layer very near the corners. Figure 17 shows contours of the magnitude of the streamwise velocity in the test section, indicating the thickness of the boundary layers on the top and bottom walls.

IV. CONCLUDING REMARKS

An analytical investigation of the flow within the contraction section of the NASA-Ames 11-ft transonic wind tunnel has been carried out. Initially, two-dimensional solutions had indicated the possibility for large secondary flows to exist as a result of the asymmetries involved in the contraction section as it is constructed. The results of a full three-dimensional solution indicate that only minor pressure variations actually occur in the contraction section within any given cross flow plane. Further analysis of the 3D solution has indicated that these slight lateral pressure gradients lead to negligible secondary flows, except within a small region in the corners within the boundary layer.

On the basis of the present solution, it would not be expected that any flow asymmetries and/or secondary flow present within the 11-ft contraction section are associated with the methods by which the contraction is implemented in its present configuration. There may be other asymmetries and variations throughout the test section flow field, however, based on the present investigation, they are probably not due to the contraction geometry itself.

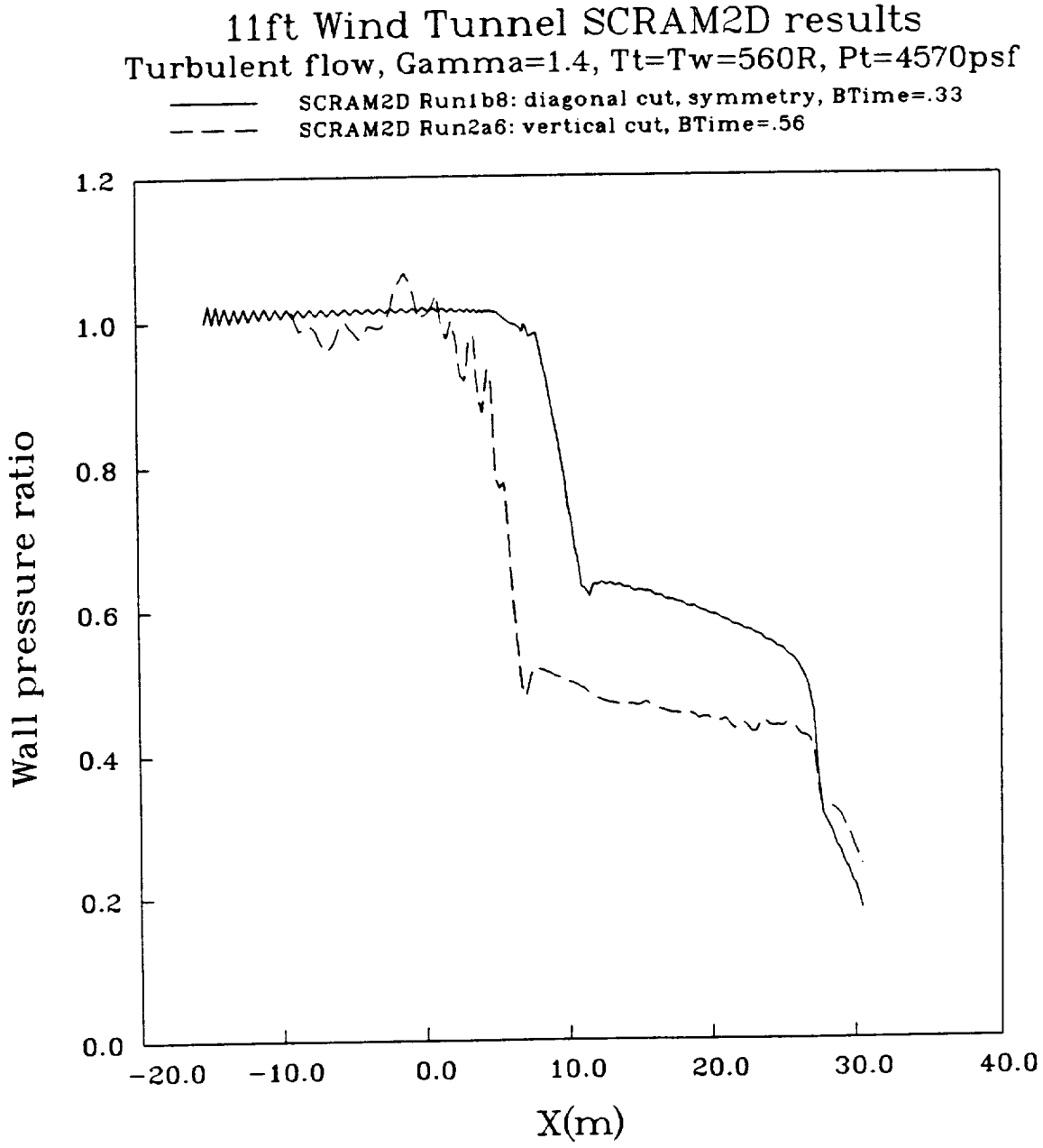

FIGURE 1. **Results of the two-dimensional calculations carried out previously showing the difference in location of the regions of favorable pressure gradient within the contraction section of the 11-foot wind tunnel.**

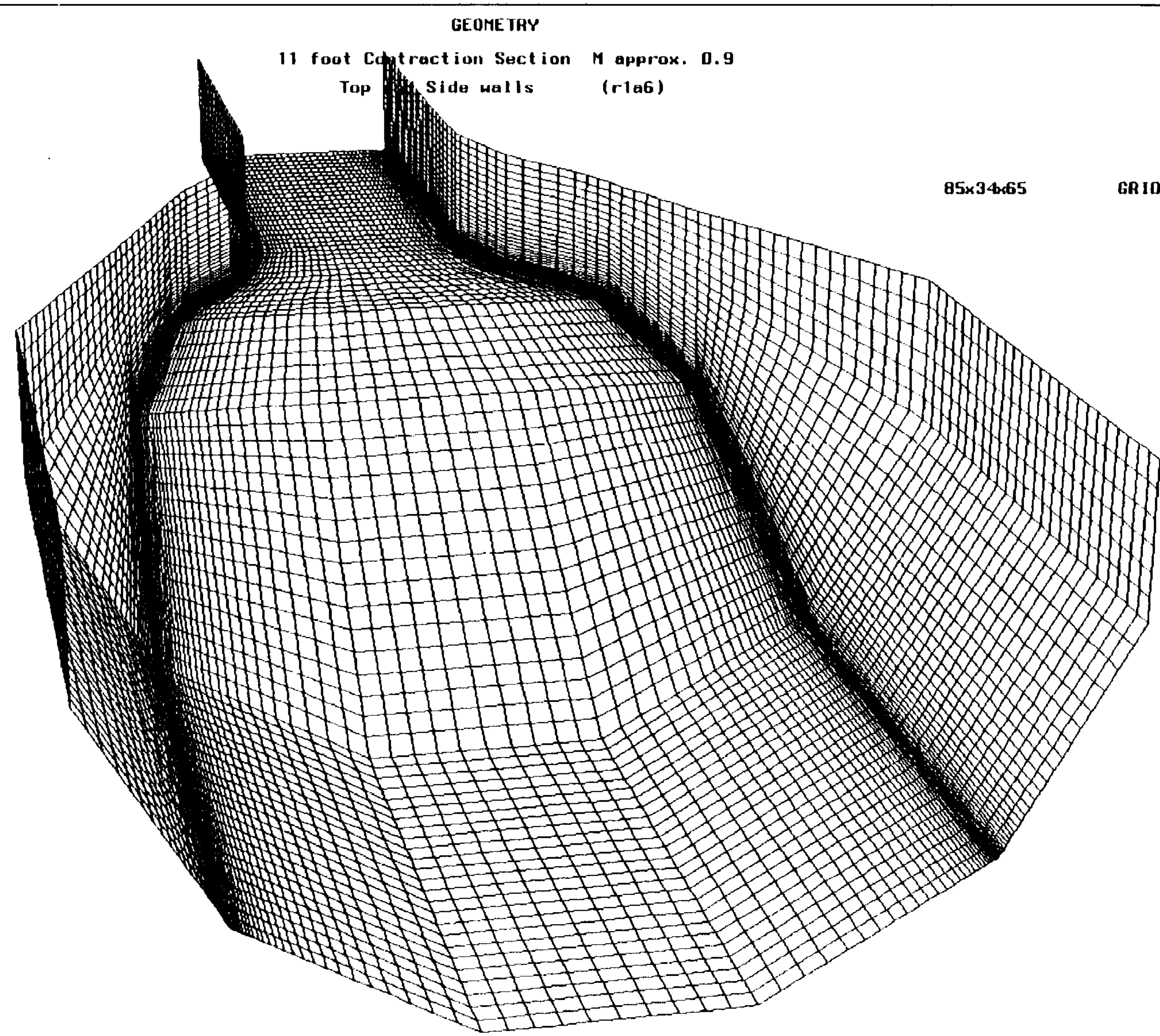

FIGURE 2. **Surface grid developed for use in the present three-dimensional calculation showing the lower half of the grid.**

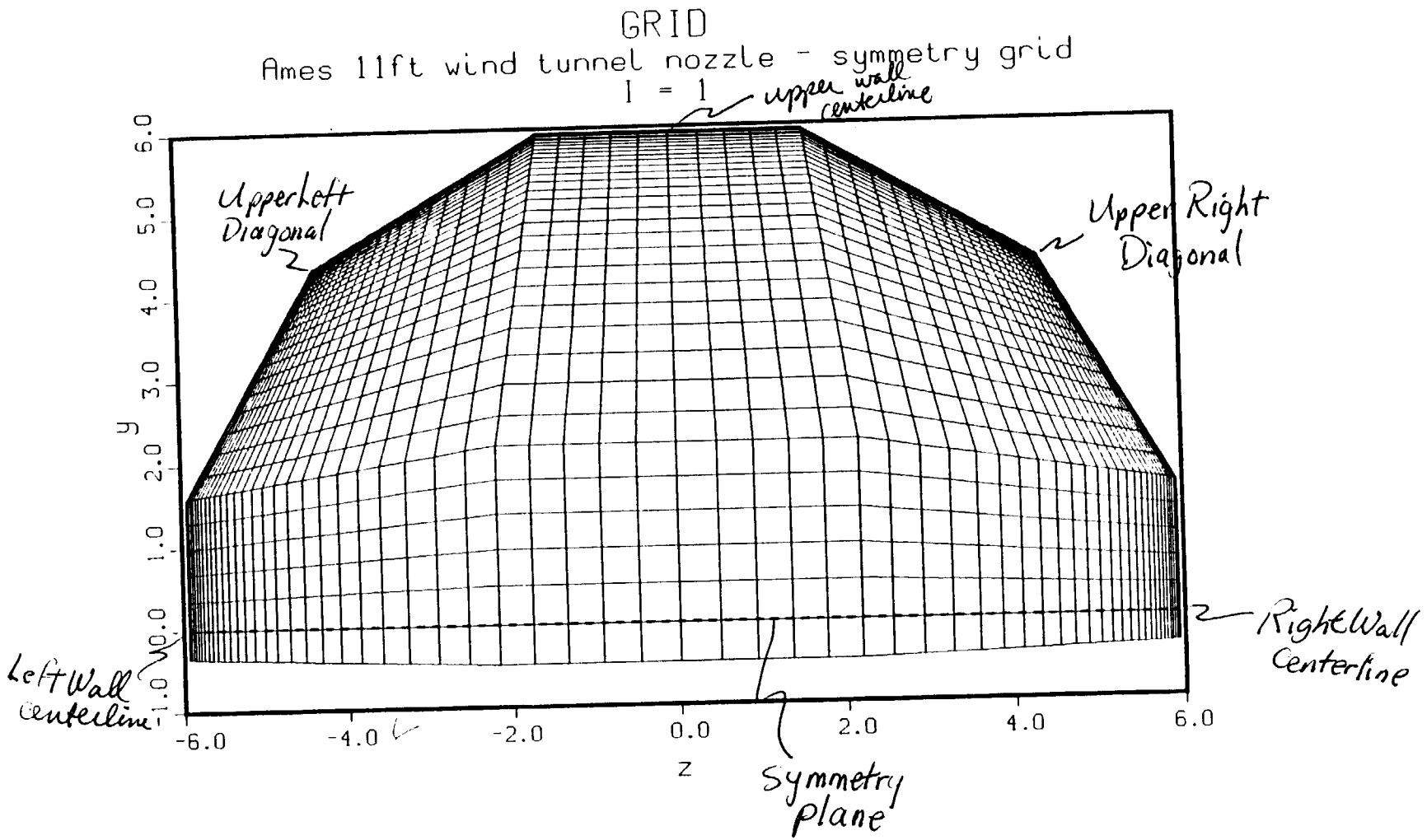

FIGURE 3. **Cross flow grid at a representative station showing the compaction of the grid near the walls.**

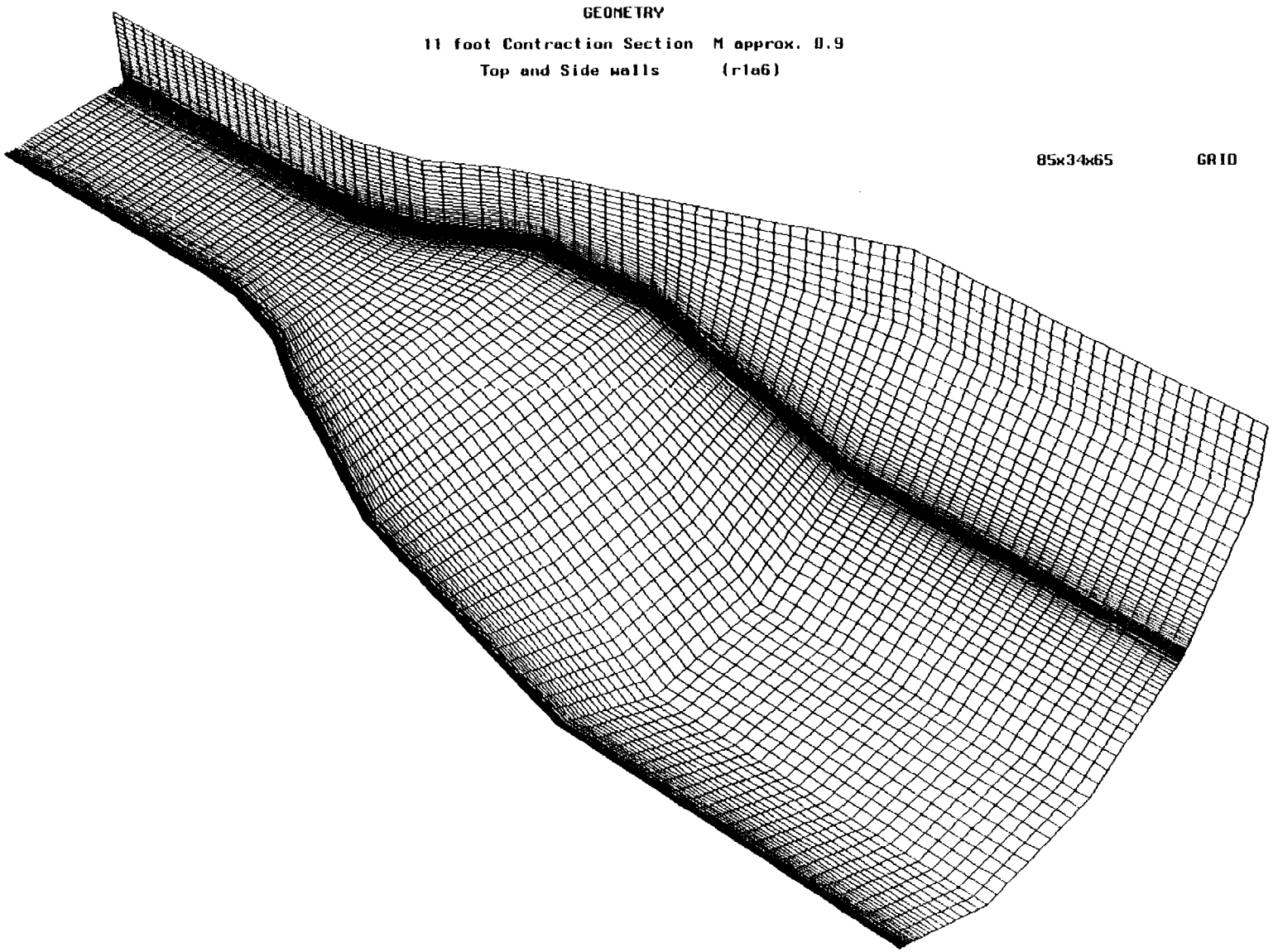

FIGURE 4. **Grid geometry in perspective used for remaining figures (position shown with the left hand (South) sidewall removed).**

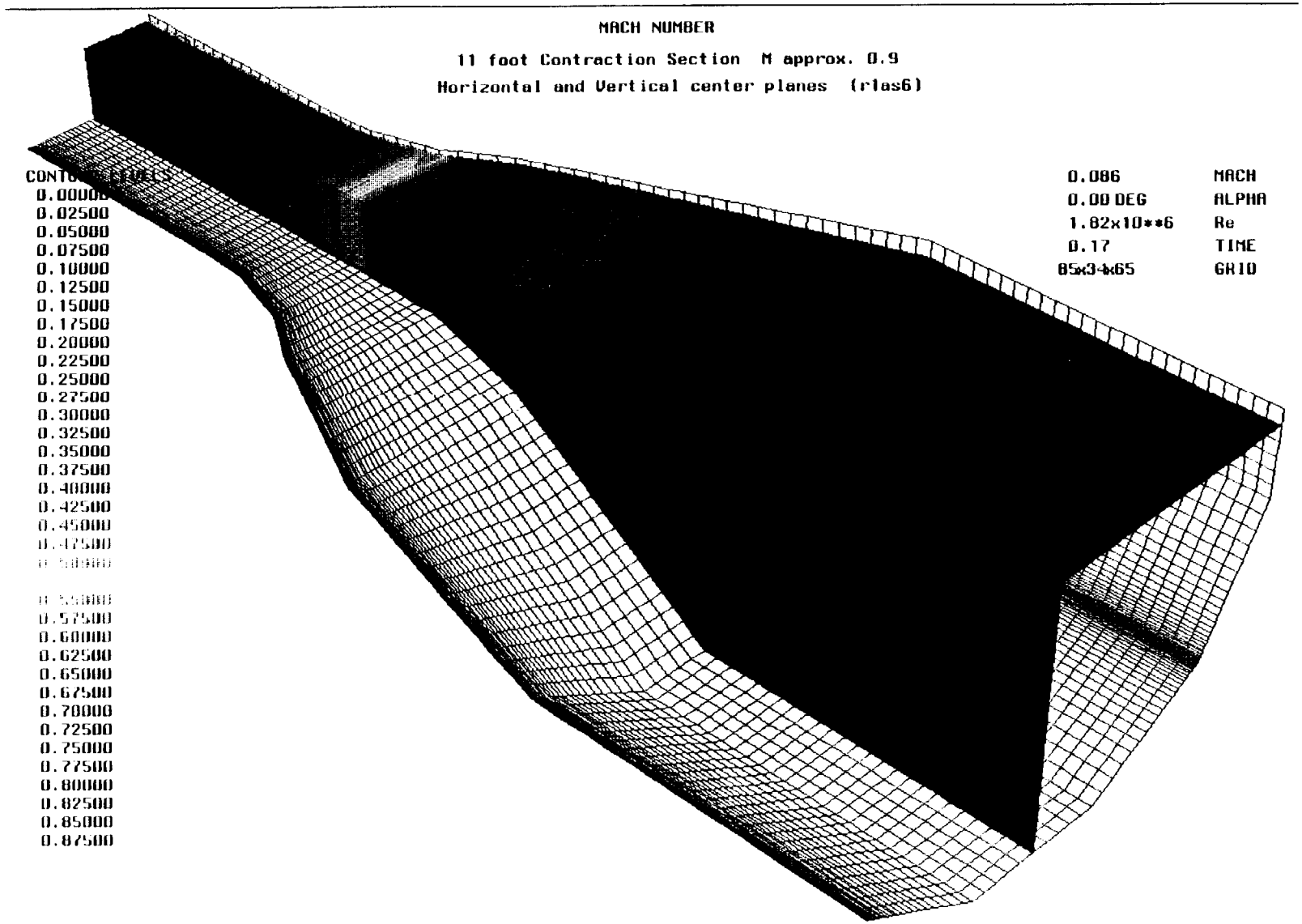

FIGURE 5. **Mach number contours shown on the vertical and horizontal symmetry planes throughout the contraction section.**

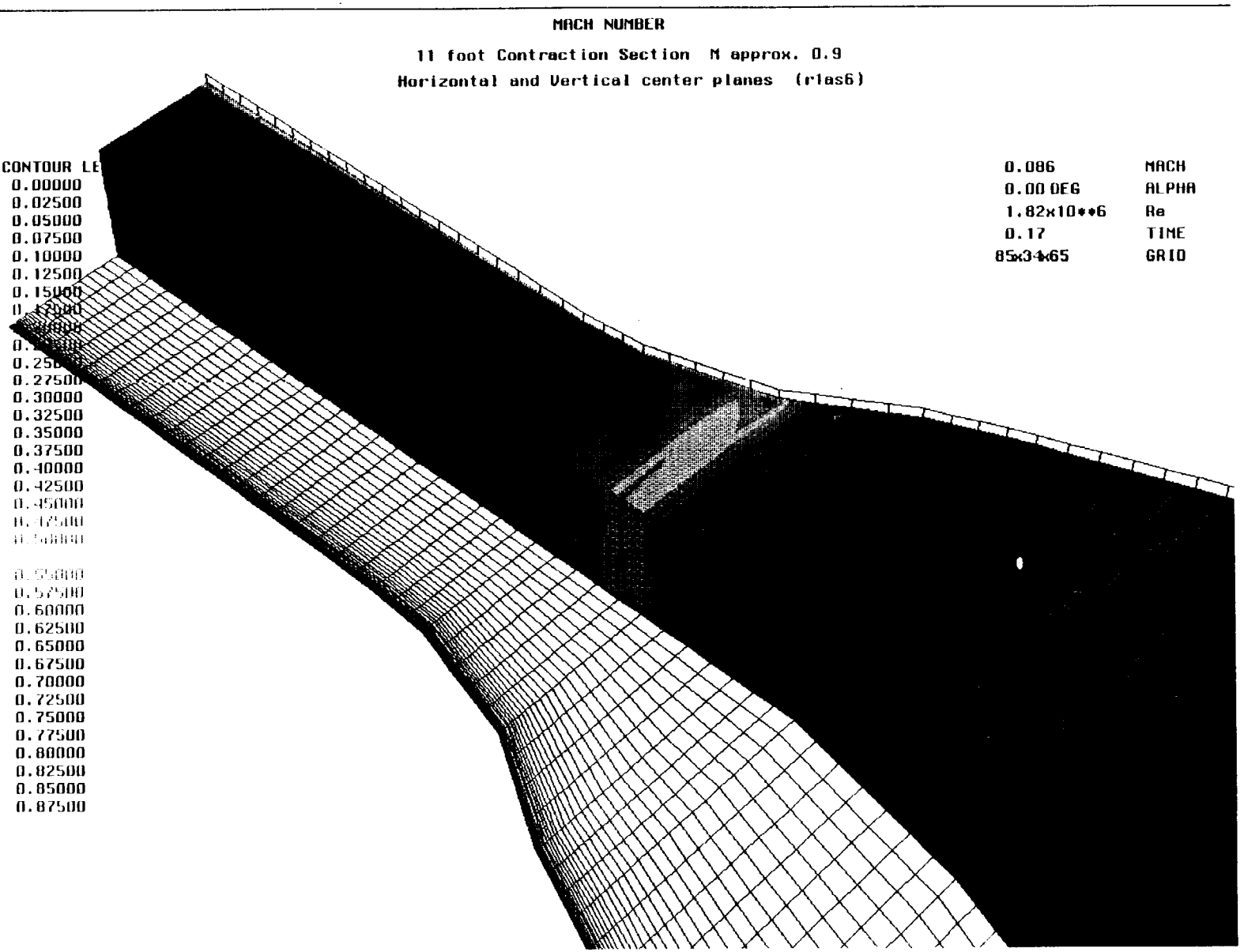

FIGURE 6. **Enlargement of the Mach number contours on the two symmetry planes showing slight variations in Mach number within the contraction section on a given cross flow plane.**

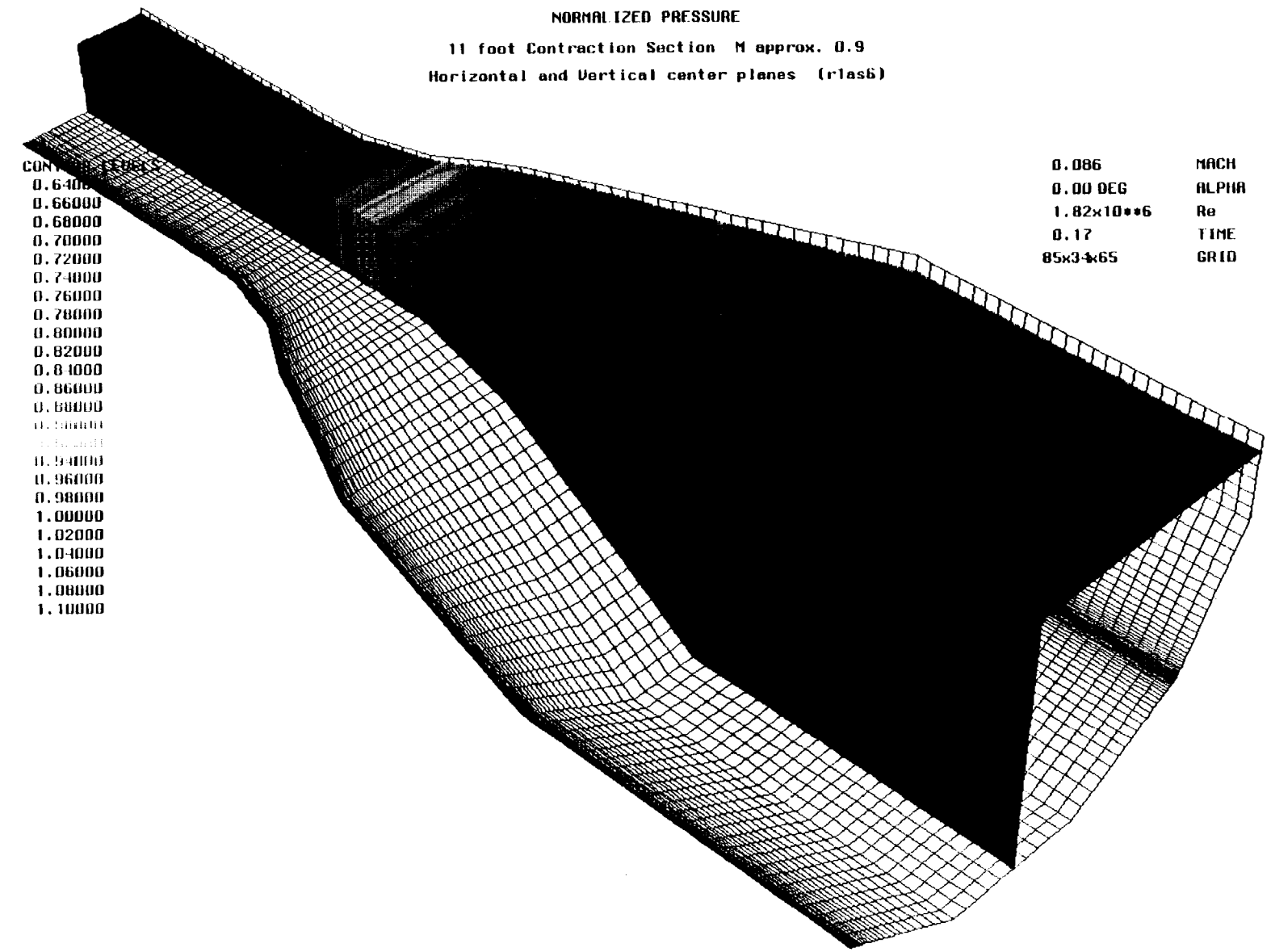

FIGURE 7. **Normalized pressure contours shown on the vertical and horizontal symmetry planes throughout the contraction section.**

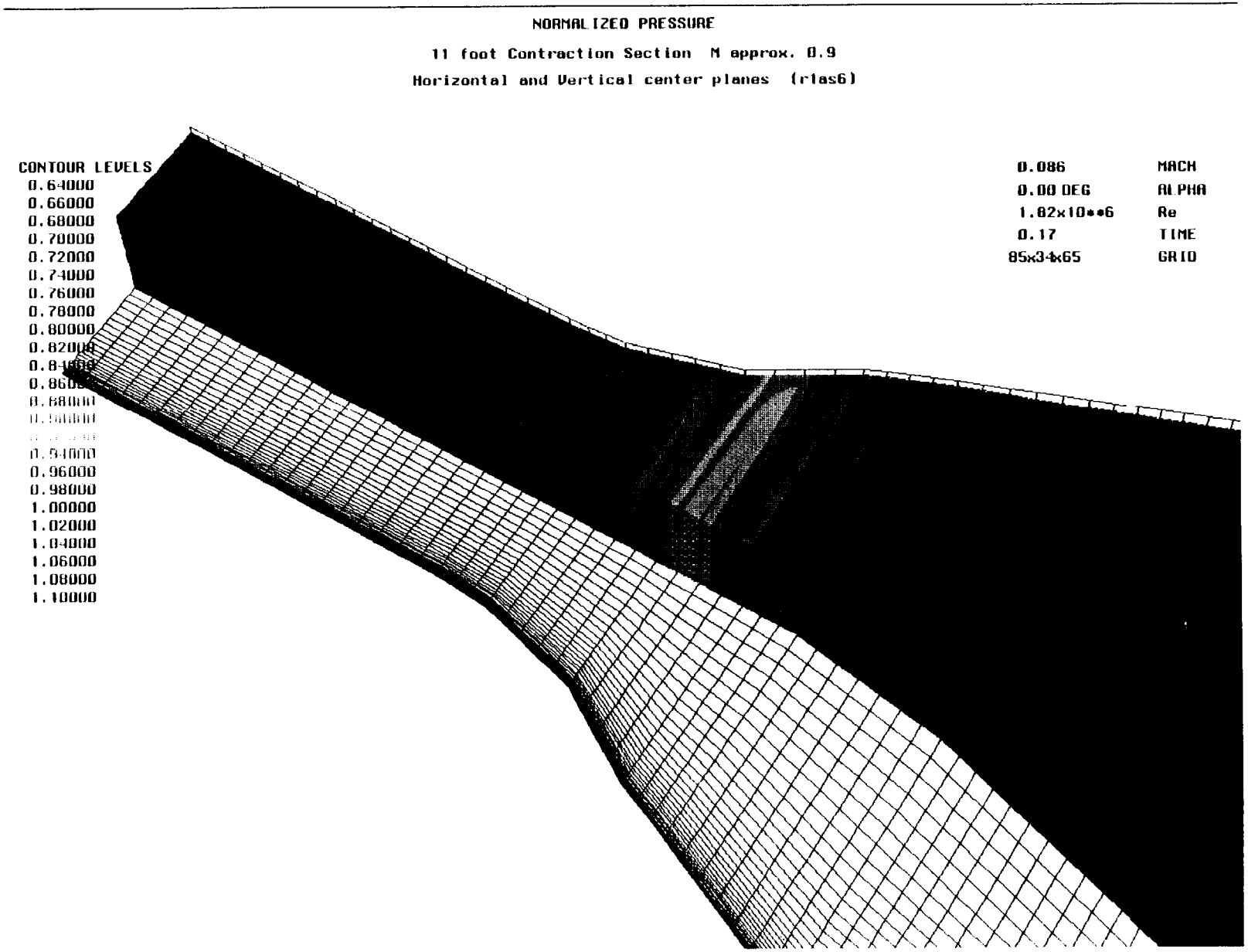

FIGURE 8. **Enlargement of normalized pressure contours showing lower pressures occurring upstream on the vertical symmetry plane than on the horizontal symmetry plane.**

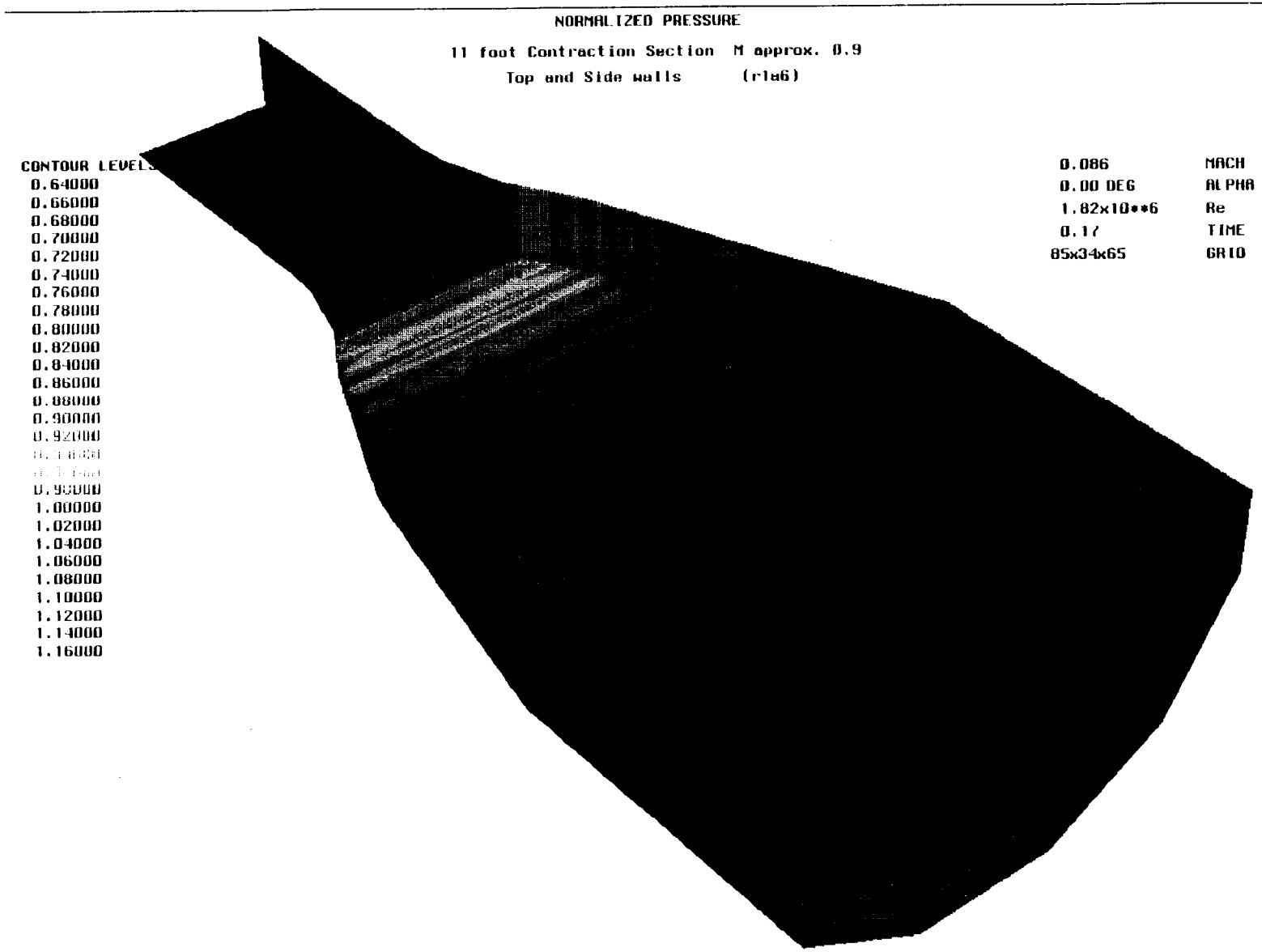

FIGURE 9. **Normalized pressure contours on the surfaces of the contraction section.**

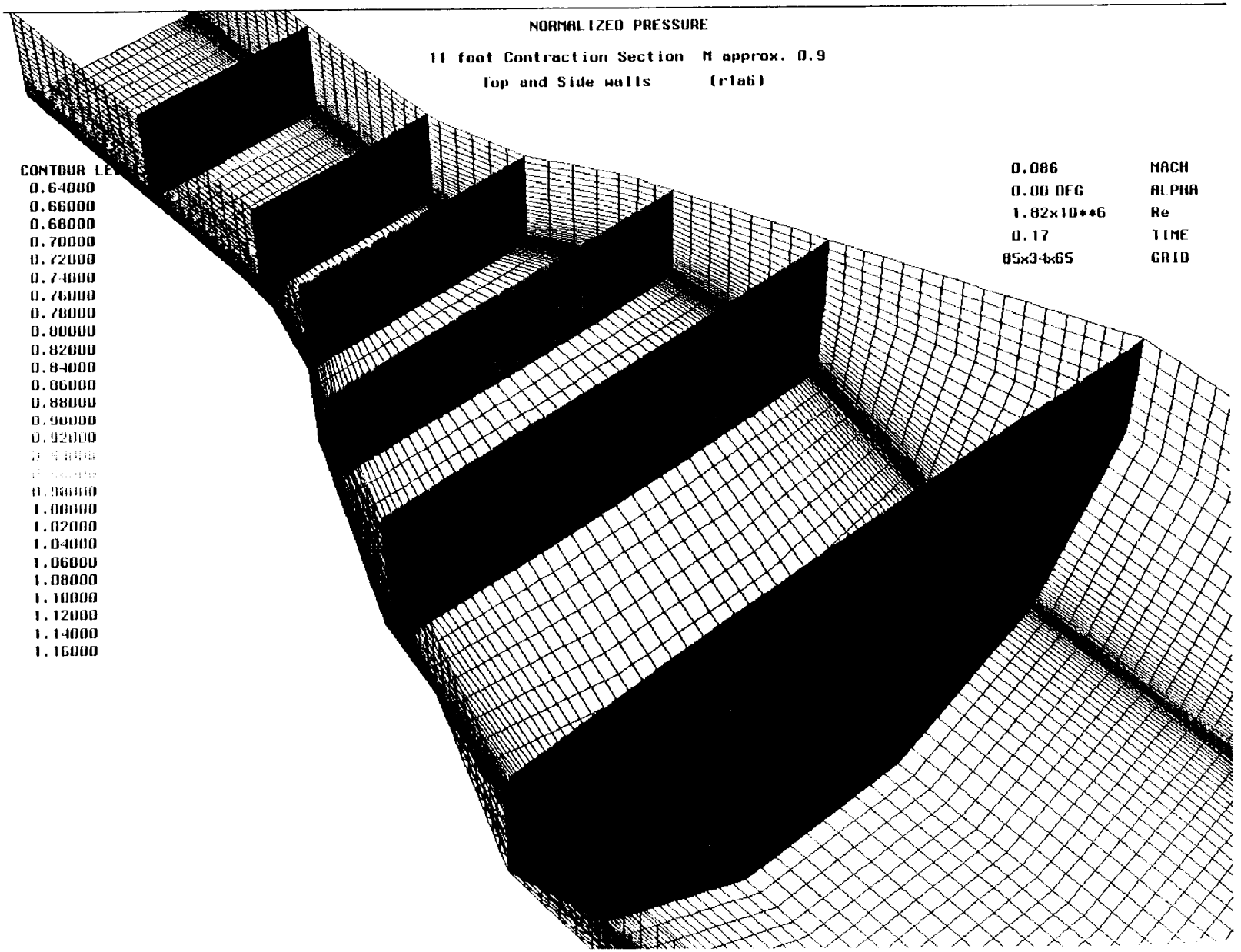

FIGURE 10. **Normalized pressure contours on 6 representative cross flow planes in the contraction section.**

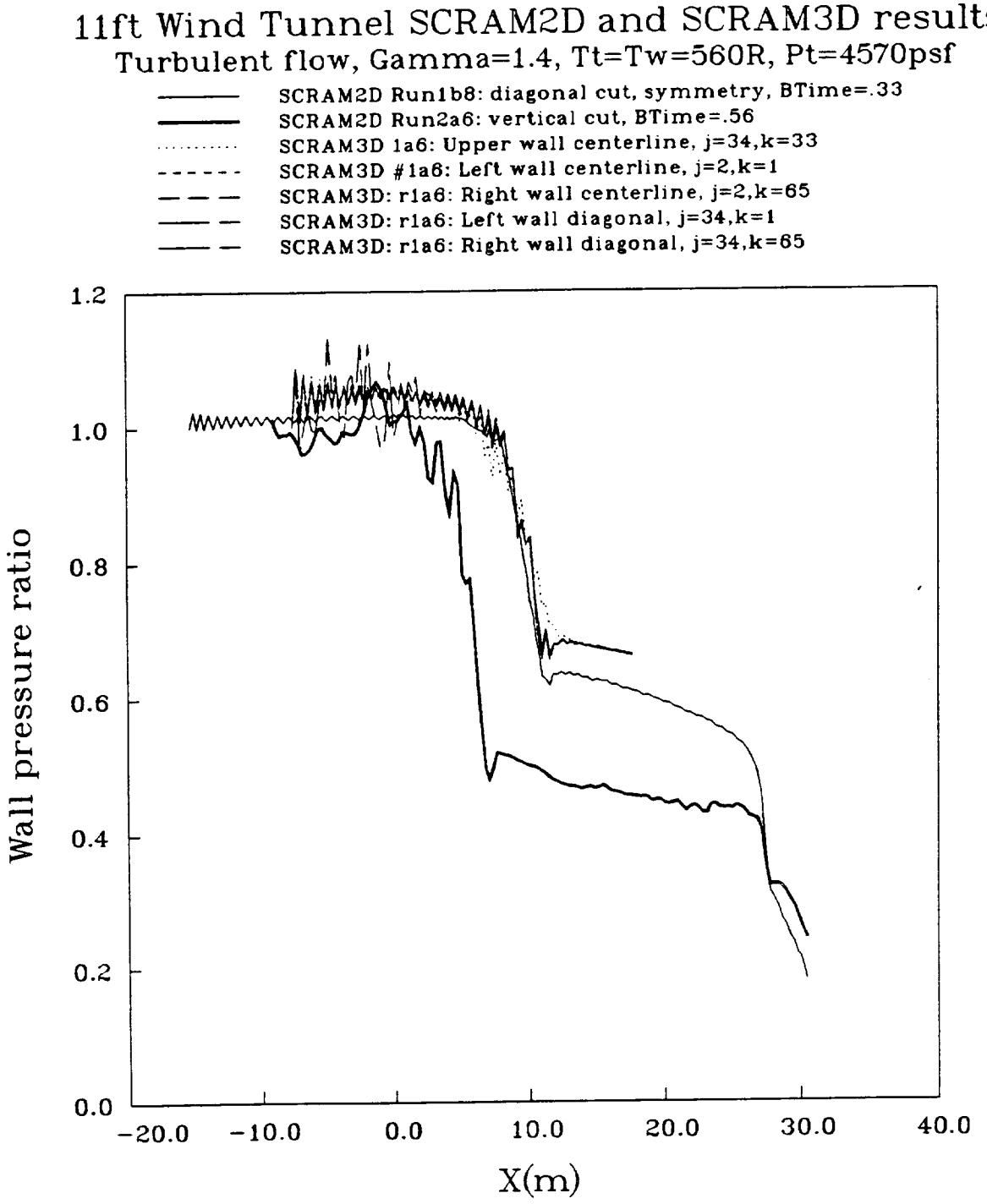

FIGURE 11. **Comparison of surface pressure distributions for two-dimensional and three-dimensional simulations through the 11-foot wind tunnel contraction.**

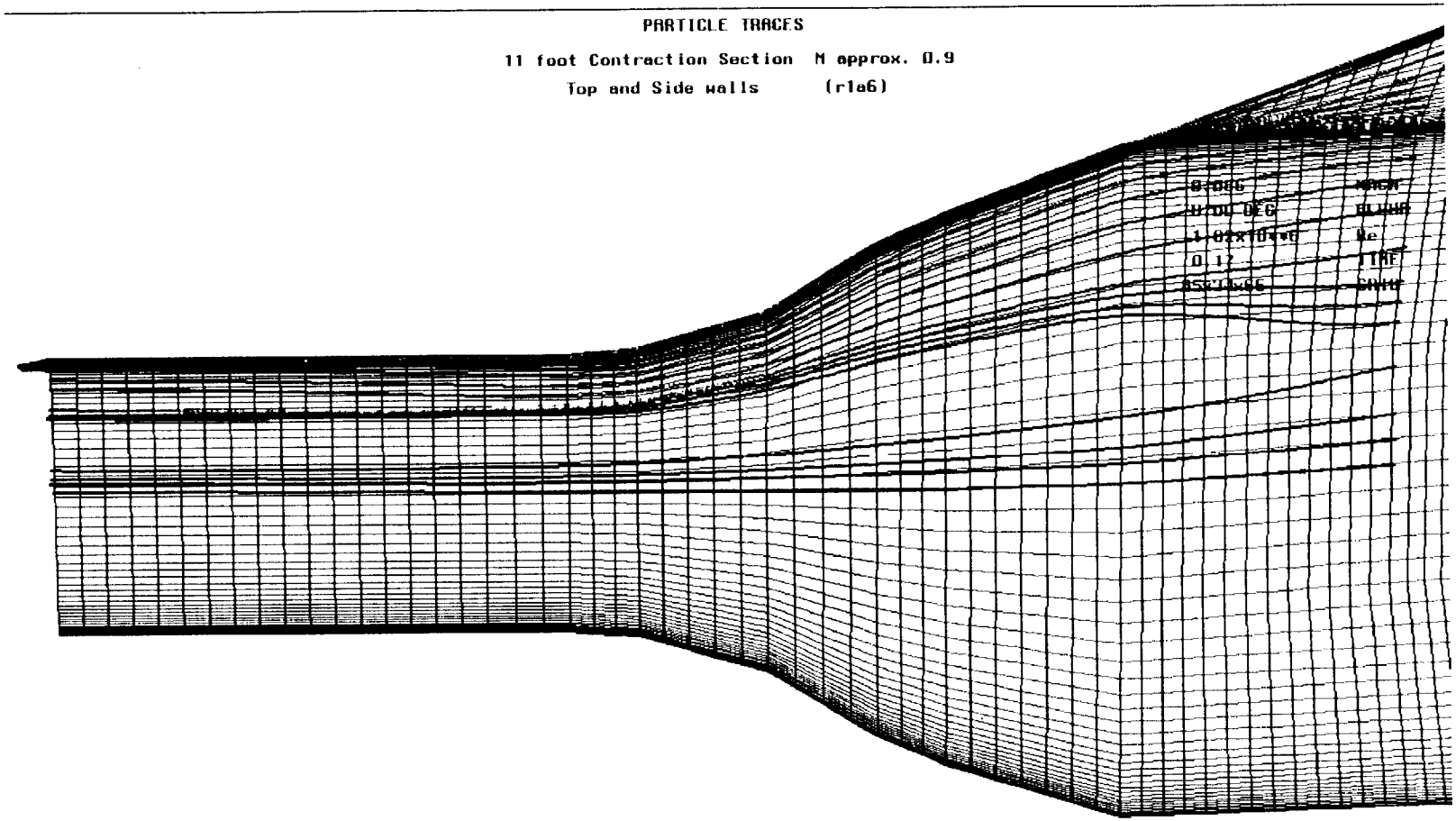

FIGURE 12. Particle traces as viewed from the top of the solution.

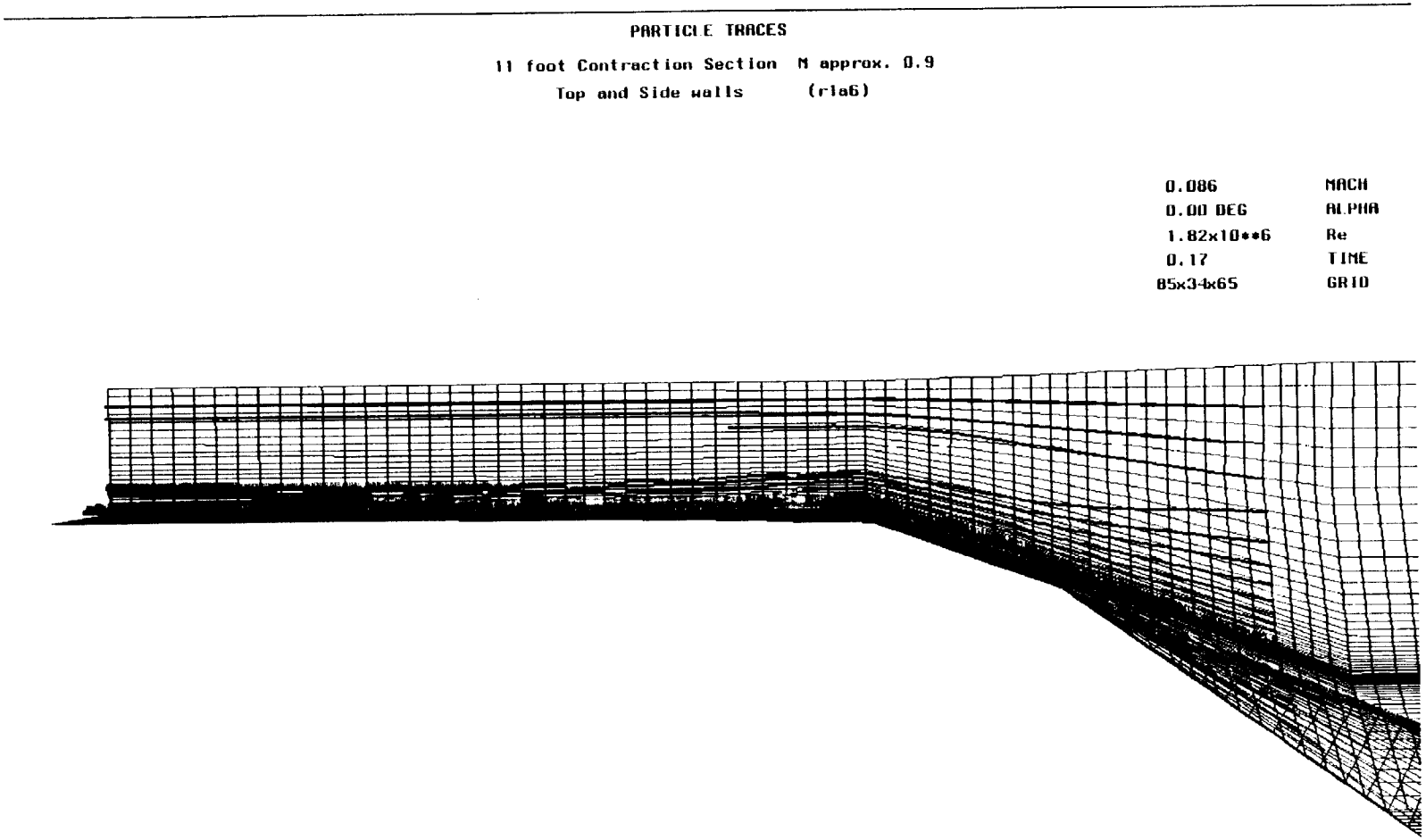

FIGURE 13. **Particle traces as viewed from the side of the solution.**

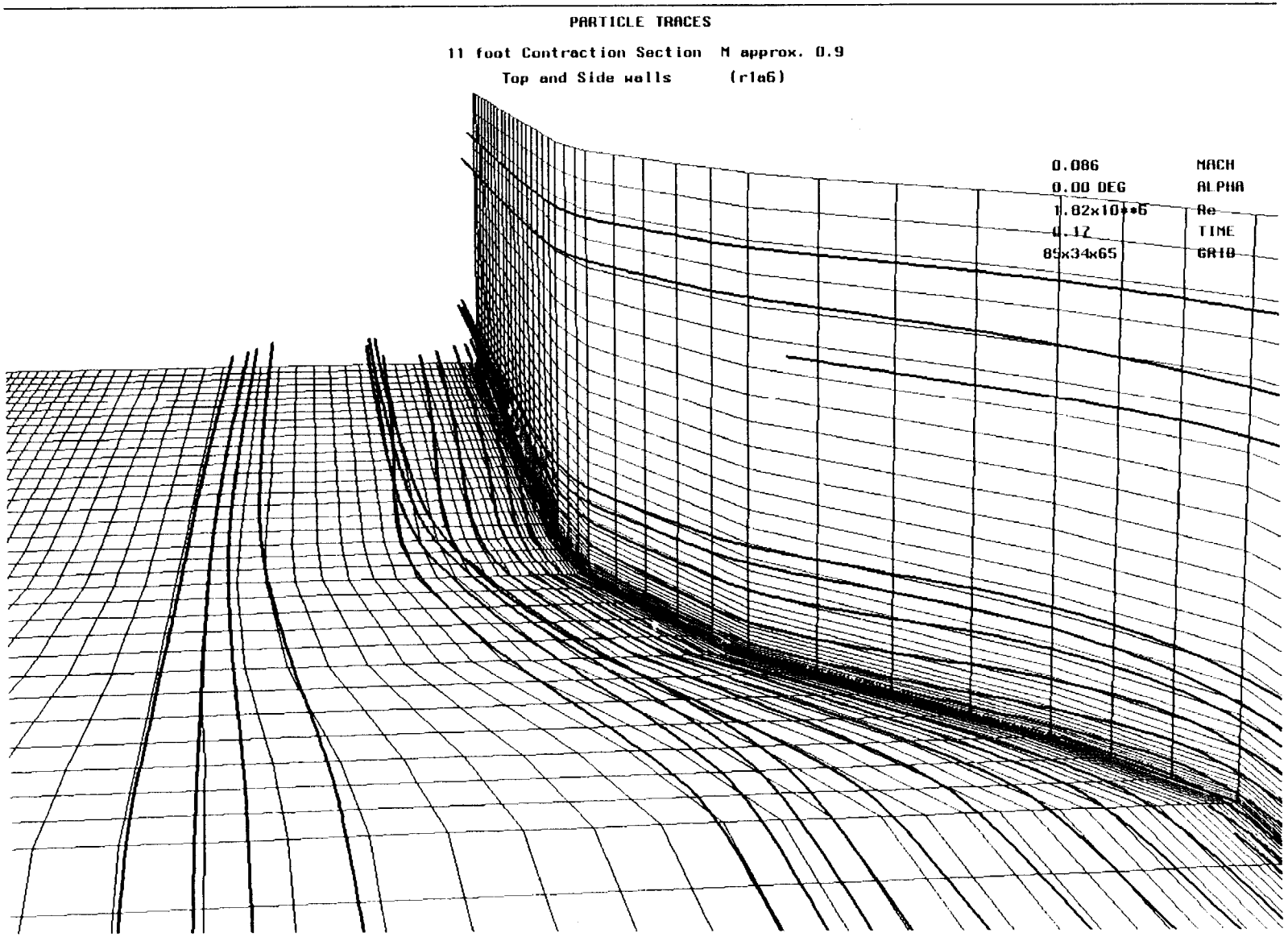

FIGURE 14. **Perspective view of particle traces released along the sidewall and bottom of the solution showing little secondary flow within the test section.**

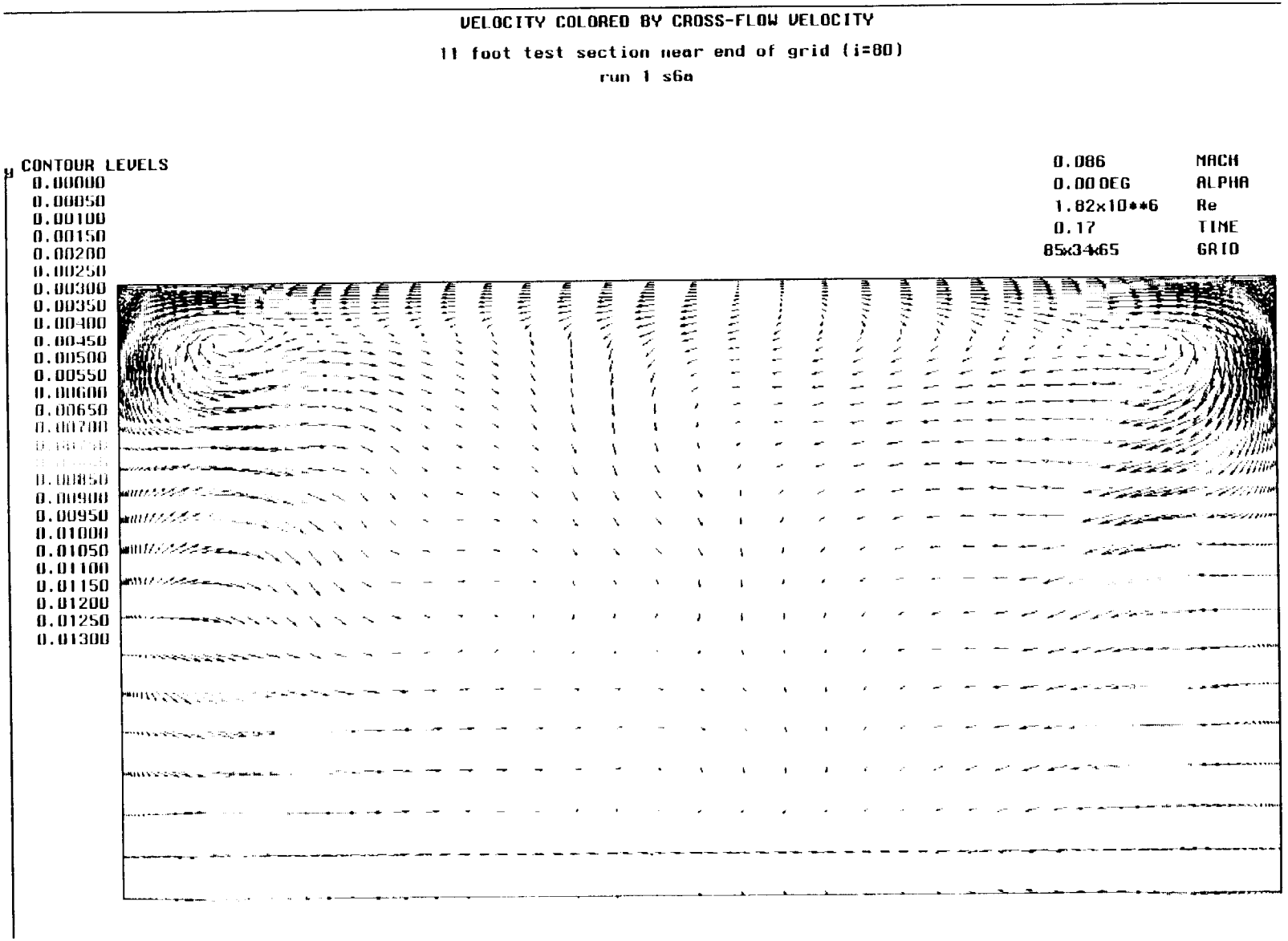

FIGURE 15. **Cross flow velocity vectors in the test section of the 11-foot wind tunnel from the 3D solution.**

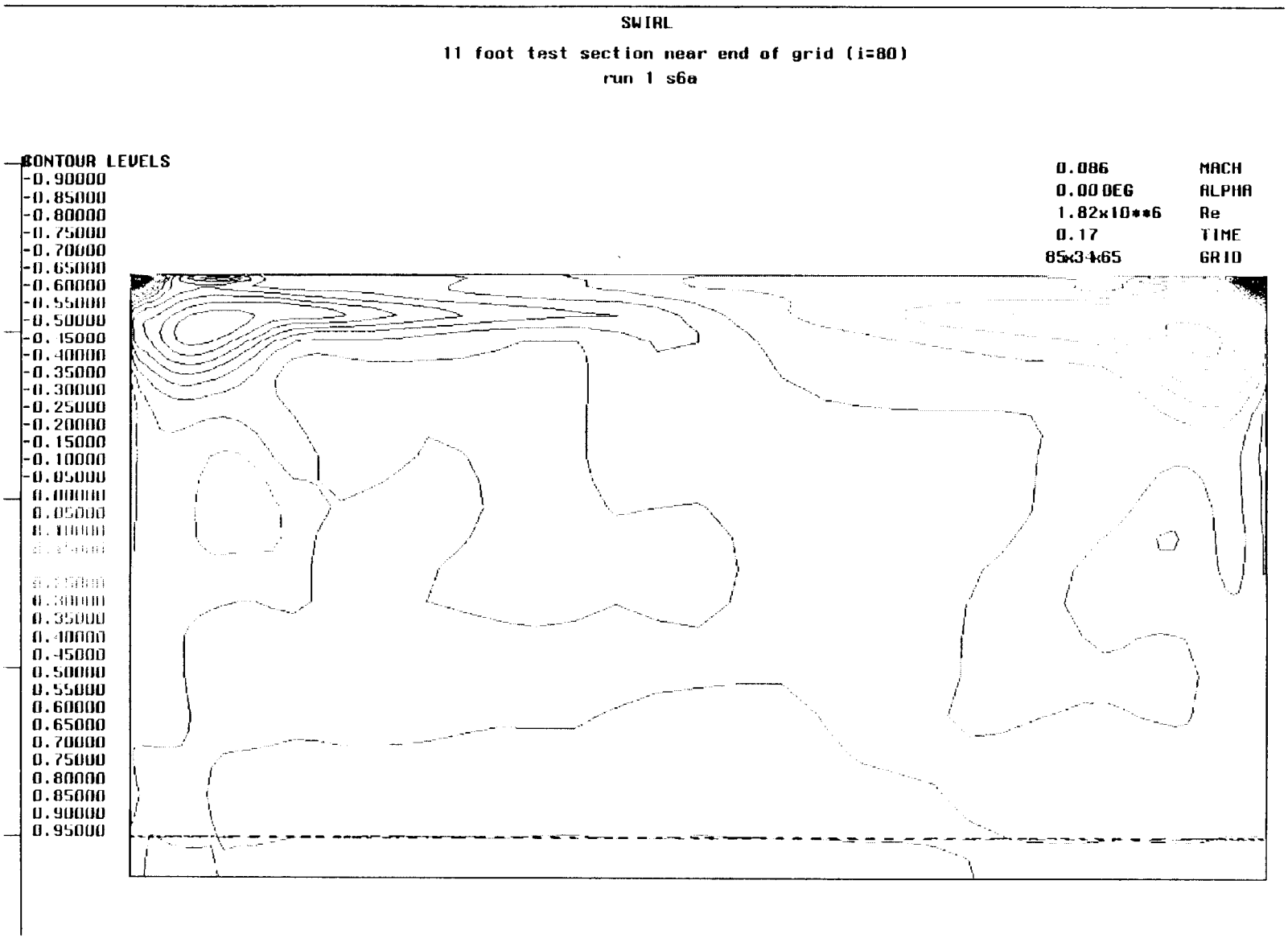

FIGURE 16. **Magnitude of the swirl in the test section of the 11-foot wind tunnel from the 3D solution.**

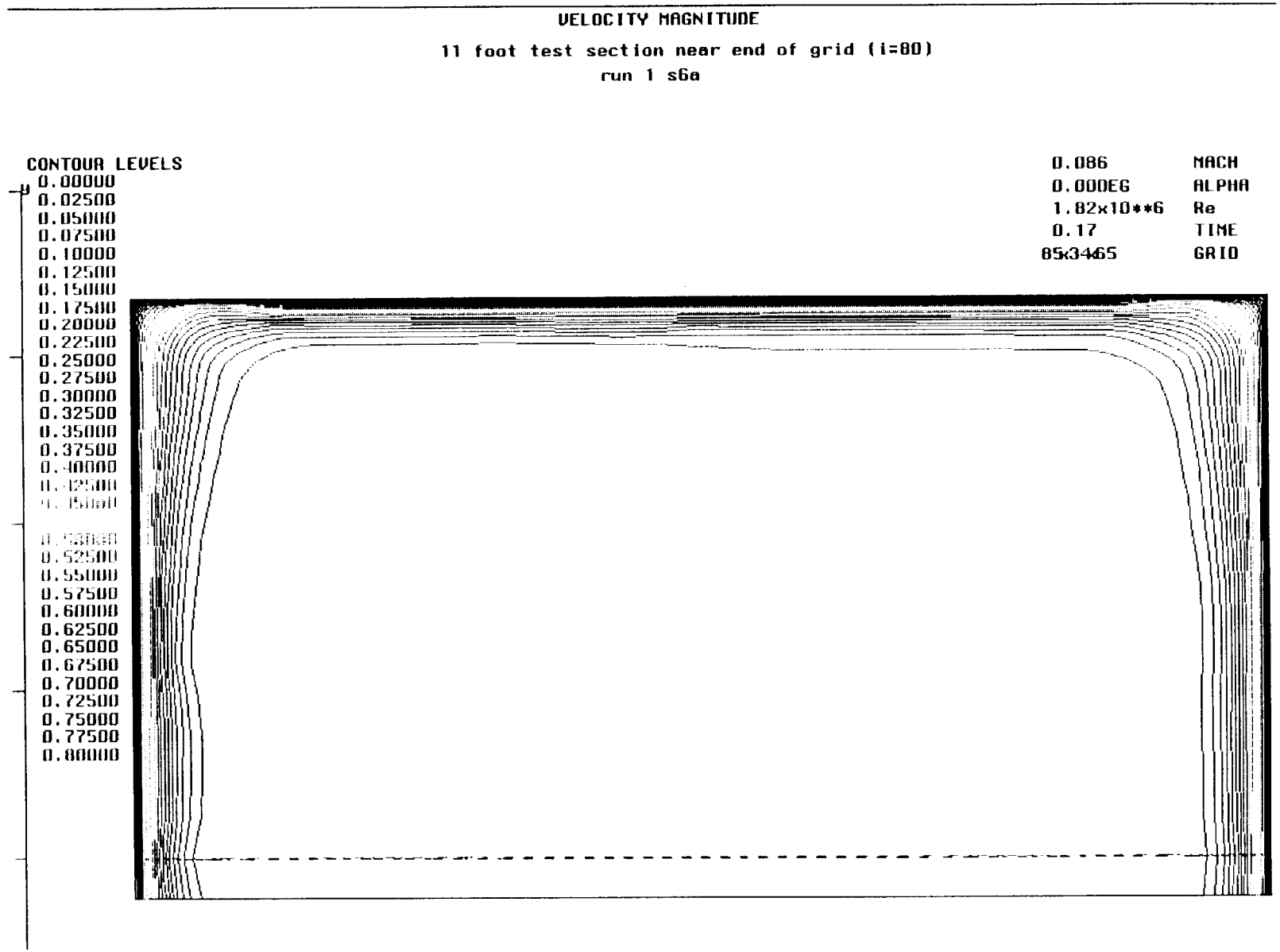

FIGURE 17. **Contours of the streamwise velocity magnitude in the test section of the 11-foot wind tunnel from the 3D solution.**